

Crystal structures of *HpSoj*–DNA complexes and the nucleoid-adaptor complex formation in chromosome segregation

Chen-Hsi Chu^{1,†}, Cheng-Yi Yen^{1,†}, Bo-Wei Chen², Min-Guan Lin², Lyu-Han Wang¹, Kai-Zhi Tang¹, Chwan-Deng Hsiao^{2,*} and Yuh-Ju Sun^{1,*}

¹Institute of Bioinformatics and Structural Biology, National Tsing Hua University, Hsinchu 300, Taiwan and ²Institute of Molecular Biology, Academia Sinica, Taipei 115, Taiwan

Received August 10, 2018; Revised August 10, 2018; Editorial Decision November 30, 2018; Accepted December 11, 2018

ABSTRACT

ParABS, an important DNA partitioning process in chromosome segregation, includes ParA (an ATPase), ParB (a *parS* binding protein) and *parS* (a centromere-like DNA). The homologous proteins of ParA and ParB in *Helicobacter pylori* are *HpSoj* and *HpSpo0J*, respectively. We analyzed the ATPase activity of *HpSoj* and found that it is enhanced by both DNA and *HpSpo0J*. Crystal structures of *HpSoj* and its DNA complexes revealed a typical ATPase fold and that it is dimeric. DNA binding by *HpSoj* is promoted by ATP. The *HpSoj*–ATP–DNA complex non-specifically binds DNA through a continuous basic binding patch formed by lysine residues, with a single DNA-binding site. This complex exhibits a DNA-binding adept state with an active ATP-bound conformation, whereas the *HpSoj*–ADP–DNA complex may represent a transient DNA-bound state. Based on structural comparisons, *HpSoj* exhibits a similar DNA binding surface to the bacterial ParA superfamily, but the archaeal ParA superfamily exhibits distinct non-specific DNA-binding via two DNA-binding sites. We detected the *HpSpo0J*–*HpSoj*–DNA complex by electron microscopy and show that this nucleoid-adaptor complex (NAC) is formed through *HpSoj* and *HpSpo0J* interaction and *parS* DNA binding. NAC formation is promoted by *HpSoj* participation and specific *parS* DNA facilitation.

INTRODUCTION

Precisely replicated DNA segregation is necessary for accurate inheritance of genetic material (1). In bacteria, the partitioning (*par*) system (ParABS) is a highly-conserved

process for the delivery and localization of chromosomes or low-copy-number plasmids in cells (2). The ParABS system comprises three elements: the NTPase motor protein (ParA: partitioning protein A); the centromere-binding protein (ParB: partitioning protein B); and a centromere-like DNA site (*parS*) (3,4). The general partitioning process involves specific binding of a *parS* site by ParB and assembly into a higher-order partitioning complex (2,4,5). The ParA dimer uses NTP-binding to trigger NTP hydrolysis, which drives segregation of newly-replicated ParB-*parS*-containing plasmids (6–8).

There are three classes of ParA NTPase motor protein: type I, a ‘deviant’ Walker-type ATPase; type II, an actin-like ATPase; and type III, a tubulin-like GTPase (8). Type I ParA can be further differentiated into types Ia and Ib depending on its structure and size (8). Type Ia ParA, such as *Escherichia coli* P1 ParA, has a non-specific DNA (nsDNA)-binding domain and a specific DNA-binding domain (9). Type Ib ParA—such as *Streptococcus pyogenes* pSM19035 Delta (δ , *SpParA*), *Salmonella newport* TP228 ParF (TP228 ParA), and *Helicobacter pylori* Soj (*HpSoj*) solely possess an nsDNA-binding domain (10–13). ParB comprises an N-terminal protein-protein interaction domain, a central helix-turn-helix DNA-binding domain, and a C-terminal self-dimerization domain (14).

Plasmid DNA stability is maintained by the ParABS system (15). In bacterial chromosome-encoded ParABS, Soj (sporulation protein J) and Spo0J (stage 0 sporulation protein J) are the homologs of the ParA and ParB proteins, respectively. In *Thermus thermophilus* and *Bacillus subtilis*, the ATPase activity of Soj is elevated by Spo0J upon addition of DNA (7,13,16). Soj exists as a monomer in the absence of ATP, but is dimeric when ATP is present. ATP-bound Soj dimer exhibits nsDNA-binding ability (7,16). Several studies have shown that DNA binding by ParA is essential for DNA segregation (17,18).

*To whom correspondence should be addressed. Tel: +886 3 574 2486; Fax: +886 3 571 5934; Email: yjsun@life.nthu.edu.tw

Correspondence may also be addressed to Dr. Chwan-Deng Hsiao. Tel: +886 2 2788 2743; Fax: +886 2 2782 6085; Email: hsiao@gate.sinica.edu.tw

†The authors wish it to be known that, in their opinion, the first two authors should be regarded as Joint First Authors.

In the ParMRC segregation system of R1 plasmid, it was found that *parC* manages plasmid molecule pairing, which requires binding of ParR to *parC*, and the ParR-*parC* pair complex is enhanced by the ParM-ATP complex (19). The DNA partitioning system of pB171 plasmid involves ParA and ParB with two *parC* sites. It has been suggested that ParB mediates the pairing complex and the higher-order complex comprising several DNA molecules, and the N-terminus of ParB was observed to be essential for ParB-mediated pair formation (20). In the *E. coli* P1 ParABS system, ParB binds to *parS* DNA to form the pairing complex (the ParB-*parS* complex) before the nucleoprotein ParA-ParB-DNA complex is assembled (15,21–23). ATP regulates these interactions and the *parS* DNA stabilizes the nucleoprotein complex (22). The dynamic interaction between plasmid-bound ParB and nucleoid-bound ParA of the ParA-ParB-DNA complex is defined as the nucleoid-adaptor complex (NAC), which mediates cooperation between the plasmid and the nucleoid (22).

Two distinct models have been proposed for the ParABS system: (i) a filament model whereby the ParB partitioning complex (i.e. cargo, the ParB-*parS* DNA complex) is translocated by ParA, which is polymerized along the nucleoid to form a nucleoprotein filament (24,25); and (ii) a diffusion-ratchet model whereby the ParB-DNA cargo is associated with ParA via a concentration gradient of ParA-ATP in the nucleoid surface (26–29). Two diffusion-ratchet mechanisms have been proposed: (a) a DNA-relay mechanism involving elastic dynamics of the chromosome involved in the translocation of the ParB partitioning cargo (30,31); and (b) a hitch-hiking mechanism whereby ParA assembles in high-density DNA regions (HDRs) to guide ParB partitioning cargo delivery (32). The diffusion-ratchet model suggests that ParA-ATP needs to undergo a conformational change into a DNA-binding competent state, ParA*₂-ATP₂, for binding to the nucleoid (26), resulting in ParA*₂-ATP₂ attachment to the nucleoid (or localization at HDRs) to form a nucleoid matrix in which the association between plasmid-bound ParB and nucleoid-bound ParA is facilitated (26,27,29,32).

Two Walker-box DNA segregation systems were identified recently in archaeal plasmids and chromosomes, i.e., SegAB and AspA-ParBA machineries (33–36). The SegAB system was characterized in the thermophilic crenarchaeon *S. solfataricus* and consists of SegA and SegB proteins and a centromere-like region (34). SegA is an ortholog of the bacterial Walker-type ATPase ParA. Similar to the polymerization behavior of bacterial ParA, SegA assembles into polymers in the ATP-bound state. Archaea SegB is a site-specific DNA-binding protein that interacts with SegA and affects SegA polymerization (34). The AspA-ParBA machinery is encoded by the plasmid pNOB8 hosted by *Sulfolobus* NOB8H2 strain (35). It comprises AspA (archaeal segregation protein A, a centromere-binding component), ParA (NTPase), and ParB (an atypical ParB) (35). Archaea AspA is a site-specific DNA-binding protein with no sequence homology to any characterized segregation protein (35). The pNOB8 ParA possesses nsDNA-binding ability (37), and a multifaceted DNA-binding mode has been identified from the structure of pNOB8 ParA-AMPPNP-DNA (37). The pNOB8 ParB exhibits nsDNA-binding activity

and functions as an adaptor protein to interact with AspA, ParA and nsDNA (35).

The crystal structure of the *HpSpo0J-parS* DNA complex of the ParABS system of *H. pylori* was previously determined (2), revealing that *HpSpo0J* molecular spreading and DNA bridging is mediated by the *HpSpo0J* N-terminus. Here, we report the crystal structures of *HpSoj* and its DNA complexes. *HpSoj* non-specifically binds to DNA through a basic binding patch comprising Lys199, Lys227, Lys230 and Lys247, and directly binds within the DNA minor groove at Asn196, Lys199 and Val229. Furthermore, we used electron microscopy (EM) to monitor nucleoprotein formation among *HpSpo0J*, *HpSoj* and DNA, allowing us to propose a potential NAC complex for the partitioning system in *H. pylori*.

MATERIALS AND METHODS

Protein expression and purification

The PCR product of the *Hp1139* (*HpSoj*) gene (795 bp) from *H. pylori* 26695 genomic DNA was ligated into the *Bam*HI and *Sal*I restriction sites of expression vector pQE30 (Qiagen) that possesses a hexa-histidine tag at the N-terminus (13). The plasmid was then transformed into the expression host, *E. coli* strain SG13009. Recombinant *HpSoj* was grown in Luria-Bertani medium and induced overnight at 20°C by adding 1 mM isopropyl-β-D-1-thiogalactopyranoside (IPTG). The Ni-NTA system (GE Healthcare) was used to purify *HpSoj* with elution buffer (20 mM Tris pH 8.0, 500 mM NaCl, 110 mM imidazole, 5 mM MgCl₂ and 10% glycerol). The eluted proteins were applied to a Superose™ 12 gel filtration column (GE Healthcare) pre-equilibrated with the elution buffer and run at 0.5 ml·min⁻¹. Molecular weight and purity of proteins were assessed by SDS-PAGE. *HpSoj* mutations (D41A, K199E, K230E, K199/230E and K199/227/230/247E) were generated by site-directed mutagenesis method and verified by DNA sequencing. Protein purification of these *HpSoj* mutants were similar to that of wild-type *HpSoj*.

PCR products of *HpSpo0J* and *HpSpo0JN* (residues 1–50) from *H. pylori* 26695 genomic DNA were ligated into the *Nco*I and *Xho*I restriction sites of the pET-28a(+) expression vector (Novagene) that contains a C-terminal hexa-histidine tag. The resulting two plasmids, pET-28a(+)-*HpSpo0J* and pET-28a(+)-*HpSpo0JN*, were transformed into *E. coli* strain BL21(DE3). The expression systems were incubated overnight at 37°C in Luria-Bertani medium. Cultures were induced by adding 1 mM IPTG and incubating at 37°C for three hours. Ni-NTA columns (GE Healthcare) were used to purify the two proteins. The eluted *HpSpo0J* and *HpSpo0JN* proteins were further purified by a Superose™ 12 gel filtration column (GE Healthcare).

DNA preparation

Double-stranded 24 and 55 bp *parS* DNA fragments were prepared using an equal molar ratio of two complementary oligonucleotides (the 16 bp *parS* site is underlined): 24 bp DNA fragment (5'-AGGGTGTTCACGTGAAACAGGGA-3') (for *parS*24), *parS*-contained 55 bp DNA fragment (5'-CTGAATCAGCAGTTGAATCAG

AATGTTCCACGTGAAACAAAGAAAAAGAA
 CCTG-3') (for *parS55*) and 55 bp DNA fragment
 (5'-CTGAATCAGCAGTTGAATCAGAATGTTT
 CACGTGAAACAAAGAAAAAGAACCTG-3') (for
 55DNA). The double-stranded DNA (dsDNA) was an-
 nealed by heating to 95°C for 30 min and then cooled
 slowly to room temperature, before being stored at 4°C
 until use.

ATPase activity assay

The ATPase activity of *HpSoj* and *HpSojD41A* was deter-
 mined using the malachite green method (38). The assay
 was performed with 4 μM (0.4 nmol) *HpSoj* or *HpSojD41A*
 and 4 mM (400 nmol) ATP in 100 μl buffer (20 mM Tris
 pH 8.0, 175 mM NaCl, 5 mM MgCl₂ and 10% glycerol)
 at 37°C for two hours. We used 4 μM (0.4 nmol) *HpSpo0J*
 or *HpSpo0JN* in the ATPase assays, with (0.4 nmol) or
 without either *parS55* or 55DNA. At various time-points
 (5, 20, 40, 60, 80, 100 and 120 min), 100 μl of the re-
 action solution was removed and immediately mixed with
 900 μl acidic coloring solution (125 mM H₂SO₄, 0.5 mM
 ammonium-molybdate, 0.01 mM ascorbic acid, 0.04 mM
 potassium antimony III oxide tartrate). The color was al-
 lowed to stabilize for 30 min before absorbances of the
 antimony-phosphomolybdate complex were detected at 850
 nm. Absorbance at 850 nm resulted from non-enzymatic
 hydrolysis of ATP was subtracted from that of each reac-
 tion mixture. We created a standard curve using a serial
 dilution of potassium phosphate (0–400 μM). *A*₈₅₀ values
 were converted into moles Pi produced per mole of pro-
 tein using phosphate absorbance as a standard. The con-
 trol experiments in the presence of DNA, *HpSpo0J* and
HpSpo0JN alone and in combination but without *HpSoj*
 were performed. The ATPase activities of these control ex-
 periments were near zero or undetectable.

Electrophoretic mobility shift assay

The DNA-binding ability of *HpSoj* was detected using
 EMSA. Reactions were performed in a volume of 24 μl in
 reaction buffer (20 mM Tris pH 8.0, 175 mM NaCl, 5 mM
 MgCl₂ and 10% glycerol). Each reaction contained *HpSoj*
 (0–1000 pmol) and *parS24* (24 bp) or *parS55* (55 bp) (25
 pmole) in various molar ratios of protein to DNA (0, 2, 10,
 20 or 40), with or without 1 mM ADP or ATP. Reactions
 were incubated at 20°C for 20 min. Samples were analyzed
 on 4–15% gradient polyacrylamide gels (GoPAGE™ TGN
 Precast Gel, SMBiO) in 1× TGN buffer at 4°C for 150 min
 and visualized by GelRed™ Nucleic Acid Gel-staining (Bi-
 otium).

Microscale thermophoresis

HpSpo0JN proteins were labeled with the fluorescent
 amine-reactive red dye NT-647-NHS (NanoTemper Tech-
 nologies) and then diluted to optimal fluorescence inten-
 sity (around 10,000 counts). Unlabeled *HpSoj* (214 μM)
 was serially diluted 1:1 in protein buffer (20 mM MOPS
 pH 7.0, 5 mM MgCl₂, 110 mM imidazole, 250 mM NaCl,
 50 mM arginine, 50 mM glutamic acid, 1 mM ATP) with

0.05% Tween20 over 16 tubes, each containing 10 μl pro-
 tein. Aliquots were mixed with 10 μl of labeled *HpSpo0JN*
 (33 nM) before being transferred into hydrophilic glass cap-
 illaries. Measurements were performed at 25°C using 20%
 LED power and 60% MST power. In the negative control
 experiment, unlabeled lysozyme (250 μM) was also serially
 diluted and mixed with labeled *HpSpo0JN*. The instrument
 used was a NanoTemper monolith NT.115Pico and the data
 were analyzed from triplicate experiments.

Crystallization

HpSoj-ATP crystals were grown using *HpSoj* (8 mg/ml)
 with an extra 10 mM ATP as an additive. The reser-
 voir solution contained Bicine pH 9.0, 8% Tacsimate,
 and 15% PEG3350. Crystals were obtained after one-
 week incubation at 10°C. *HpSoj*-ADP-DNA crystals were
 grown at a 2:1 molar ratio of *HpSoj* and *parS24* (5'-
 AGGGTGTTCACGTGAAACA GGGA-3', underlined
 is the *parS* site). The reservoir solution contained 50 mM
 MES pH 5.6, 240 mM KCl, 10 mM MgCl₂, and 6%
 PEG8000. *HpSoj*-ADP-DNA crystals were grown at room
 temperature over 3 days. *HpSoj*-ATP-DNA crystals were
 grown at a 5:1 molar ratio of *HpSoj* and *parS24*, and the
 reservoir solution contained 50 mM MES pH 5.6, 200 mM
 KCl, 10 mM MgCl₂ and 4% PEG8000. Crystals of *HpSoj*-
 ATP-DNA were obtained within one day following incu-
 bation at 20°C.

Fluorescence polarization binding isotherms

The equilibrium DNA binding assays of *HpSoj* was done by
 fluorescence polarization binding isotherms. *parS24* DNA
 substrates were fluorescently labeled on the 5' end of DNA,
 which are enabled to measure the increase in fluorescence
 polarization of the *HpSoj*:DNA complex relative to the
 unbound DNA due to *HpSoj* binding. Serial dilutions of
HpSoj proteins were made in 20 mM Tris-HCl pH 8.0, 175
 mM NaCl, 5 mM MgCl₂, 10% glycerol and 1 mM ATP be-
 fore being incubated with 5 nM Cyanine-3 (Cy3)-labeled
 DNA at room temperature. DNA binding by *HpSoj* was
 determined by measuring the changes in fluorescence polar-
 ization using a Paradigm plate reader (Molecular Devices).
 Fluorescence polarization (FP) signal was read at 595 nm at
 an excitation of 535 nm and calculated by determining the
 concentration of *HpSoj* required to bind 50% of the Cy3-
 labeled DNA. The unbound state is represented by the fluo-
 rescence anisotropy of the Cy3-labeled DNA in the presence
 of buffer alone. The experiments of *HpSoj* mutant proteins
 (K199E, K230E, K199/230E, K199/227/230/247E) were
 performed as that of wild-type *HpSoj*. The average of three
 independent experiments is shown, with error bars repre-
 senting standard deviations.

Data collection and structure determination

X-ray diffraction data for the *HpSoj*-ATP, *HpSoj*-ATP-
 DNA and *HpSoj*-ADP-DNA crystals were collected in the
 Super Photon ring-8 GeV (SPring-8), Japan, and the Na-
 tional Synchrotron Radiation Research Center (NSRRC),
 Taiwan. All datasets were processed by the HKL-2000 soft-
 ware (39).

Table 1. X-ray diffraction data and refinement statistics of *HpSoj* and *HpSoj*-DNA complexes

Crystal	<i>HpSoj</i> -ATP	<i>HpSoj</i> -ADP-DNA	<i>HpSoj</i> -ATP-DNA
Data collection statistics			
Source	Spring-8 44XU	NSRRC-TPS05A	NSRRC-TLS15A
Wavelength (Å)	0.90000	1.00000	1.00000
Space group	P2 ₁ 2 ₁ 2 ₁	P1	P1
Resolution (Å)	1.9	2.5	3.4
Unit cell parameters			
<i>a</i> (Å)	48.1	74.8	74.4
<i>b</i> (Å)	93.3	74.7	74.6
<i>c</i> (Å)	110.9	80.7	80.4
α (°)	90.0	71.5	71.4
β (°)	90.0	71.6	71.6
γ (°)	90.0	67.7	67.8
Number of reflections	181 905	97 062	32 909
Number of unique reflections	37 426 (3776)	49 136 (5041)	18 173 (2049)
Redundancy of reflection	4.9	2.0	2.0
Completeness (%), overall	93.6 (96.3)	96.0 (97.9)	88.0 (98.6)
<i>I</i> / σ (<i>I</i>), overall	23.7 (3.9)	13.4 (1.5)	8.5 (2.0)
<i>R</i> _{merge} ^b (%), overall	7.3 (37.2)	5.0 (37.4)	13.3 (41.9)
Refinement statistics			
Resolution (Å)	30.0–1.9	29.8–2.5	26.8–3.4
<i>R</i> -factor ^c / <i>R</i> _{free} ^d (%)	16.6/20.2	20.4/24.7	20.1/25.0
Number of reflections used	36,400	49,125	17,784
Number of residues	528	1,056	1,056
Number of atoms			
Protein	4106	8208	8208
DNA	-	984	984
ATP	62	108 (ADP)	124
Mg	2	4	4
Water	494	19	0
<i>B</i> -factor (Å ²)			
Protein	21	59	85
DNA	-	98	120
ATP	14	41 (ADP)	73
Mg	11	49	70
Water	29	-	-
RMSD bond lengths (Å)	0.008	0.017	0.012
RMSD bond angles (°)	1.267	1.928	1.698
PDB ID ^e	6IUB	6IUD	6IUC

^aValues in parentheses are for the highest-resolution shell.

^b $R_{\text{merge}} = \sum |I - \langle I \rangle| / \sum I$, where *I* is the observed intensity and $\langle I \rangle$ is the average intensity from multiple observations of symmetry-related reflections.

^c $R = \sum |F_{\text{obs}} - F_{\text{calc}}| / \sum F_{\text{obs}}$, where *F*_{obs} and *F*_{calc} are the observed and calculated structure factor amplitudes, respectively.

^d*R*_{free} was calculated with 5% of the total number of reflections randomly omitted from the refinement.

^eProtein data bank identifiers for co-ordinates.

The structural phases of *HpSoj*-ATP were determined by molecular replacement (MR) with Phaser (40), using *TtSoj* (PDB ID: 1WCV) (7) as a search model. Structural phases of *HpSoj*-ATP-DNA and *HpSoj*-ADP-DNA were solved by MR using *HpSoj* as the search model. Structural refinements were performed in Phenix (41), and structural model adjustment was carried out in COOT (42). X-ray diffraction data and structural refinements are summarized in Table 1.

Electron microscopy

For electron microscopy, *parS550* (550 bp DNA with one *parS* site in middle), 180DNA (180 bp DNA) and 600DNA (600 bp DNA) were used. The *parS550*, 180DNA, and 600DNA fragments were amplified by PCR. The DNA-only control (Supplementary Figure S5) was examined by a Cytochrome C spreading technique (43). For the *HpSpo0J:parS550* complex, we used 20 nM *HpSpo0J* and 2 nM *parS550* in binding buffer (20 mM Tris pH 8.0, 150 mM NaCl, 5 mM MgCl₂, 33 mM imidazole, 10% glyc-

erol). For the *HpSoj*:180DNA complex, we used 80 nM *HpSoj* and 4 nM 180DNA in the presence of ATP (1 mM). *HpSpo0J* and *parS550* DNA (molar ratio 10:1), *HpSpo0J* and 600DNA (molar ratio 10:1), or *HpSoj* and 180DNA (molar ratio 20:1) were incubated for 10 min at 37°C. To induce NAC formation, the *HpSpo0J-parS550* complex and the *HpSoj*-180DNA complex were mixed together and incubated for 6 h at 37°C. The resulting protein-DNA mixture was placed on a clean Parafilm surface and was picked up on a carbon-coated grid before being negatively stained with 1% uranyl acetate. After the grid had been air-dried for one day, rotary shadowing was performed with the platinum-palladium source at an angle of 10 degree and a sample-to-source distance of 8 cm. The grid was coated with carbon and then visualized by electron microscopy. Images were captured by a Tecnai G2 Spirit TWIN (FEI Company) electron microscope at a magnification of $\times 15\,000$ at 80 kV. EM image quantifications were conducted using ImageJ. Image frames were randomly selected from different grids. The *parS550*, 180DNA, and 600DNA fragments were dis-

Table 2. The counts and number of *HpSpo0J*-DNA, *HpSoj*-DNA and *HpSpo0J*-*HpSoj*-DNA

	Protein: <i>parS550</i> complex	Protein: <i>parS550</i> paired complex	Protein: <i>parS550</i> :180DNA complex	Higher-order Complex	Molecules Counted, % (n)
[<i>HpSpo0J</i> : <i>parS550</i>]	70.9% (144)	12.8% (26)	-	16.3% (33)	100% (203)
[<i>HpSpo0J</i> : <i>parS550</i>]+[<i>HpSpo0J</i> :180DNA]	85.3% (174)	6.4% (13)	1.5% (3)	6.9% (14)	100% (204)
[<i>HpSoj</i> : <i>parS550</i>]+[<i>HpSoj</i> :180DNA]	90.9% (140)	5.8% (9)	3.2% (5)	0.0% (0)	100% (154)
[<i>HpSpo0J</i> : <i>parS550</i>]+[<i>HpSoj</i> :180DNA]	72.3% (125)	6.9% (12)	18.5% (32)*	2.3% (4)	100% (173)

*Nucleoid-adaptor complex (NAC) formation.

tinguishable by length. Numbers of various complexes in images are listed in Table 2 and Supplementary Table S3.

RESULTS

Characterization of *HpSoj*

HpSoj belongs to the ParA superfamily. We present a multiple sequence alignment in Supplementary Figure S1 of the ParA superfamily from the bacterial *par* system (7,9,11,16,25) and of archaeal *Sulfolobus* NOB8H2 pNOB8 ParA (35). *HpSoj* shares a sequence identity of 22–48% with the ParA superfamily. In addition, proteins of the ‘deviant’ Walker A motif family with different biological functions (44–47) are also shown in Supplementary Figure S1. *HpSoj* shares a sequence identity of 18–28% with the ‘deviant’ Walker A motif superfamily.

We assayed the ATPase activity of *HpSoj* by the malachite green method (37) (Figure 1A). *HpSoj* achieved ATP hydrolysis of 1.0 ± 0.3 moles Pi released/mole *HpSoj*·hour⁻¹. The activities show slightly increase of 1.4- and 1.3-fold with specific DNA (*parS55*) and non-specific DNA (55DNA), respectively. However, the ATPase activity of *HpSoj* with *HpSpo0J* reveals an increase of 3.8-fold using *parS55* but only 1.2-fold with 55DNA. The ATPase activity of *HpSoj* was stimulated when *HpSpo0J* binds to *parS55* and the *HpSpo0J*-*parS* complex is formed. In addition, the ATPase activities of *HpSoj* were detected by *HpSpo0JN* (the N-terminal domain only of *HpSpo0J*) with 3.7- and 3.1-fold stimulation in *parS55* and 55DNA, respectively (Figure 1A). Although *HpSpo0JN* does not contain the DNA binding domain it still can stimulate the ATPase activity of *HpSoj*. It suggested that *HpSpo0JN* enhances ATP hydrolysis of *HpSoj*. In addition, we conducted the MST experiment to detect the potential interaction between *HpSoj* and *HpSpo0JN* and a weak interaction was observed (Figure 1B).

We assessed the DNA-binding ability of *HpSoj* by EMSA using *parS24* and *parS55* fragments and with or without nucleotide ADP or ATP (Figure 1C and Supplementary Figure S2). We found that the DNA-binding ability of *HpSoj* is dependent on ATP. The DNA-binding were observed under ATP and ADP, at the concentrations of *HpSoj* of 0.4 and 1.5 mg/ml, respectively (Figure 1C and Supplementary Figure S2). Meanwhile, *HpSoj* completely bound DNA at a molar ratio of 40:1 in the presence of ATP (Figure 1C).

Overall structure of *HpSoj*

HpSoj exhibits Rossmann folding, which is a typical of nucleotide-binding protein (Figure 2A), and forms a dimer

(Figure 2B). *HpSoj* comprises a central seven-stranded β -sheet ($\beta 1$ – $\beta 7$) framed by $\alpha 1$ – $\alpha 2$ and $\alpha 9$ – $\alpha 11$ on one side and $\alpha 3$ – $\alpha 8$ on the other side (Figure 2A). The ATP molecule in complex with the hexa-coordinated magnesium ion was wedged into a surface-exposed cavity formed by helices $\alpha 1$ and $\alpha 9$ and loops $\beta 1\alpha 1$ and $\alpha 8\alpha 9$ (Figure 2A). Each *HpSoj* monomer binds to one ATP that is sandwiched between the interfaces of the dimer (Figure 2B). The ATP is bound to loop $\beta 1\alpha 1$ (residues 11–19) of the conserved Walker A motif, and is shielded from the other monomer by loop $\beta 6\alpha 7$ (residues 155–158) (Figure 2B). However, the highly conserved Lys12 residue of the neighboring monomer can interact with the ATP by extended hydrogen bonding (Supplementary Table S1). In addition, Gly13 and Gly14 from the neighboring monomer make van der Waal contacts with the ATP molecule (Supplementary Table S1). *HpSoj* forms a tight dimer with a buried surface area of 1440 Å², as calculated by PISA (48) (Figure 2B). Dimerization of *HpSoj* involves seven hydrogen bonds and numerous hydrophobic interactions (Supplementary Table S2). Based on the crystal structures of ParA superfamily, there are also several hydrogen bonds and hydrophobic interactions existed in *TtSoj*, *SpParA* and TP228 ParA dimer interface. However, the conservation among these dimerization residues is low.

We further characterized the ATP molecule in the *HpSoj*-ATP structure by the $F_o - F_c$ omit map (Figure 2C), and found that its binding pocket mainly comprises $\alpha 1$ and loop $\beta 1\alpha 1$ (Walker A motif), loop $\beta 2\alpha 2$ (Walker A' motif) and $\beta 5$ (Walker B motif), as well as $\beta 6$, $\alpha 9$ and loops $\beta 5\alpha 6$, $\beta 6\alpha 7$, $\alpha 8\alpha 9$ (Figure 2A and Supplementary Figure S1). The ATP is completely trapped between the interfaces of the *HpSoj* dimer by numerous interactions (Figure 2C and Supplementary Table S1). The magnesium ion is hexa-coordinated with Thr18, ATP O1B, ATP O3G, and three water molecules (Supplementary Table S1c).

According to previous reports on *Soj* (7,10), a key functional aspartic acid residue (Asp41 in *HpSoj*) co-ordinates the water nucleophile (W_{Nu}) and initializes ATP hydrolysis, playing an important role in ATPase activity. Asp41 of *HpSoj* binds the W_{Nu} and interacts with the γ -phosphate of ATP to initiate ATP catalysis (Figure 2C), as found for Walker-type ATPases. The ATP-binding residues are all conserved and critical in the ParA superfamily (7,16), and corresponding residues in *HpSoj* are ¹⁴GVGKTT¹⁹ (the ‘deviant’ Walker A motif), Asp41, and Asp130 (Figure 2C). The ATP hydrolysis of *HpSojD41A* was reduced to 0.4 ± 0.2 mol Pi released/mole *HpSojD41A*·hour⁻¹. The P1 ParAD152N and *TtSojD44A* (corresponding to *HpSojD41A*) also have been reported and *TtSojD44A* mu-

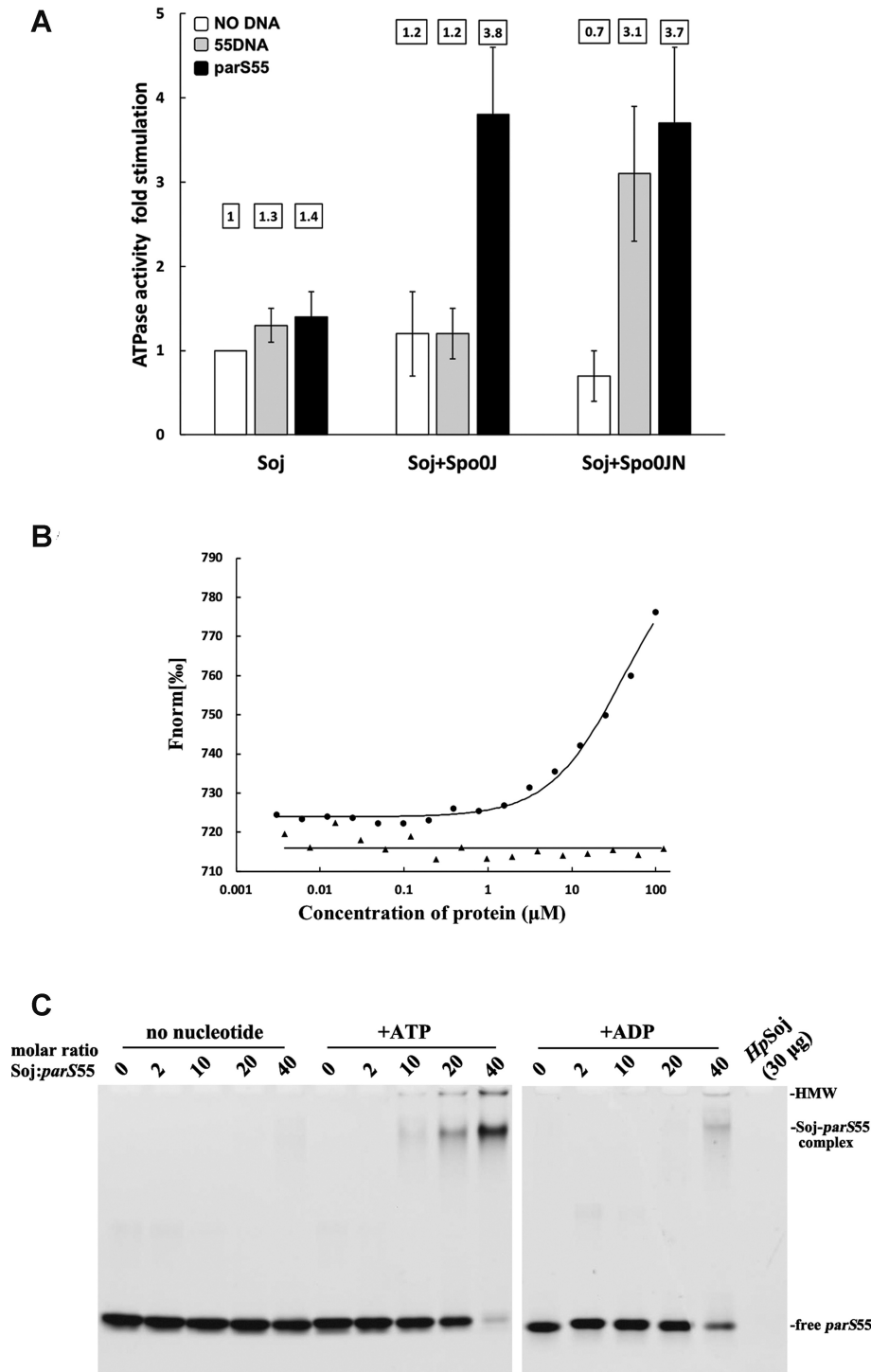


Figure 1. *HpSoj* characterization. (A) ATP hydrolysis. The purified *HpSoj* derivatives were incubated with ATP in reaction mixtures containing 55DNA, *parS55*, *HpSpo0J* derivatives or both. The released inorganic phosphate (Pi) was detected spectrophotometrically. Non-enzymatic hydrolysis of ATP was undetectable, and the resulting absorbance was subtracted from that of each reaction mixture. Fold stimulation was calculated by setting the ATP hydrolysis rate of *HpSoj* as one. Error bars represent the standard error of the mean ($n = 3$). (B) Microscale thermophoresis binding measurements of *HpSoj* and *HpSpo0JN*. The labeled *HpSpo0JN* were mixed with serially diluted *HpSoj* (●) or lysozyme (▲) which was used as a negative control. (C) EMSA of *HpSoj* DNA binding. *HpSoj* binds *parS55* in a concentration-dependent fashion in the presence of ATP, but binding is weak at a protein to *parS55* molar ratio of 40:1 in the presence of ADP. HMW – high molecular weight.

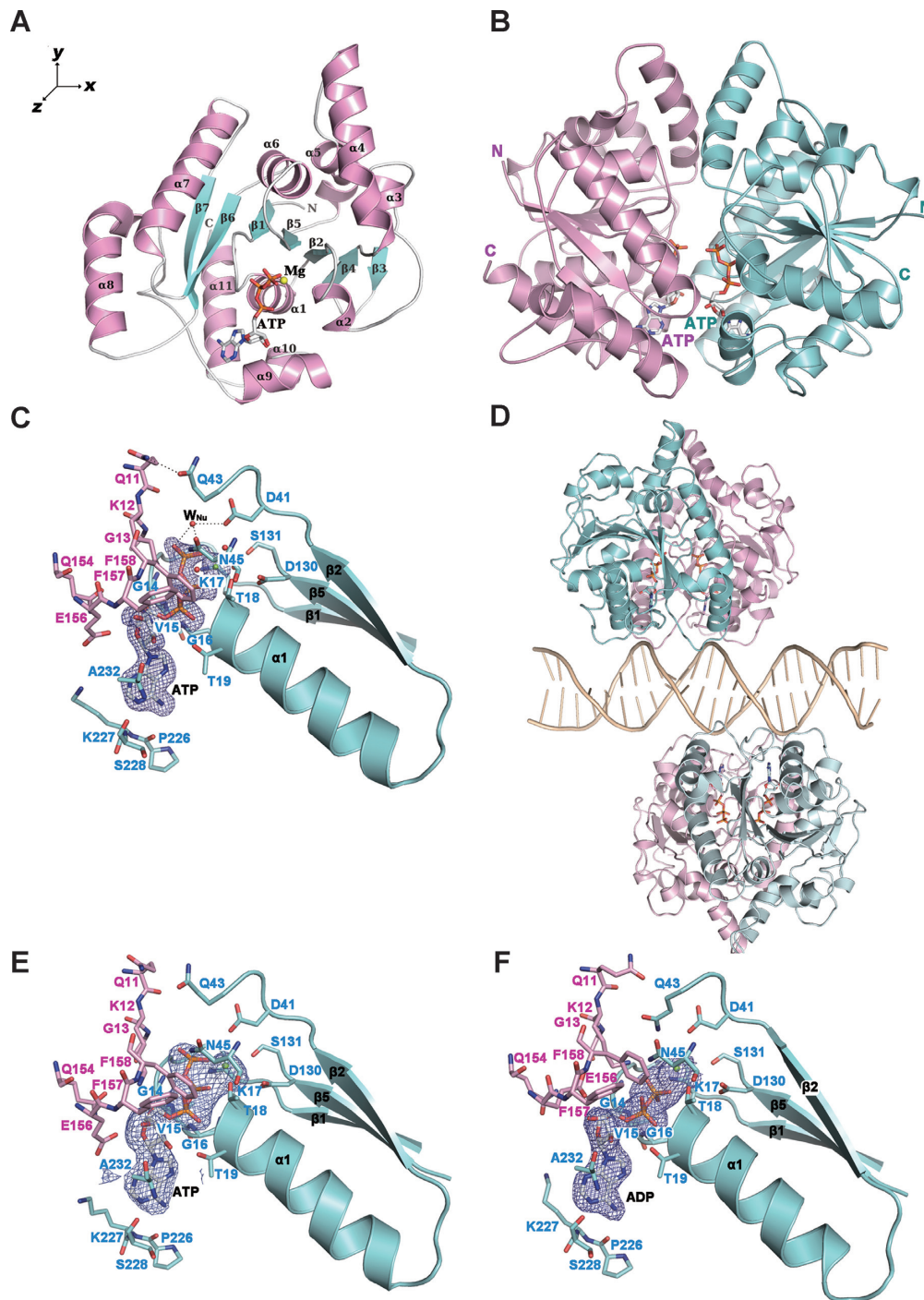


Figure 2. Crystal structures of *HpSoj*-ATP and its DNA complexes. (A) *HpSoj* monomer. The structure of *HpSoj*-ATP monomer comprises eleven α -helices ($\alpha 1$ - $\alpha 11$) and seven β -strands ($\beta 1$ - $\beta 7$). ATP is shown as a stick and the magnesium ion is shown as a yellow sphere. (B) *HpSoj* dimer. The two monomers of the dimer are colored in magenta and cyan, respectively. The monomer colored in magenta is rotated 90° along the y -axis relative to the monomer shown in (A). (C) The ATP-binding site of the *HpSoj*-ATP complex. (D) The *HpSoj*-ATP-DNA complex. The overall structure of the *HpSoj*-ATP-DNA complex is shown as a ribbon model. The monomers of the dimer are colored in magenta or cyan, respectively. The DNA molecule bound to the two dimers is colored pale orange. The ATP-binding sites of (E) the *HpSoj*-ATP-DNA complex and (F) the *HpSoj*-ADP-DNA complex. In (C), (E) and (F), the $F_o - F_c$ omit electron density maps of ATP and ADP are contoured at 3.0σ and shown as a mesh. The ATP/ADP-interaction residues from two monomers of the dimer are shown as sticks and are colored magenta and cyan, respectively. Water molecules in the ATP-binding pocket are shown as red spheres, and the nucleophilic water molecule is labeled as W_{Nu} . The magnesium ion is shown as a yellow-green sphere. Hydrogen-bond interactions are shown as dashed lines.

tant was suggested as an ATP-hydrolysis deficient mutant (7,49).

HpSoj–DNA complexes

The overall structure of the *HpSoj*–ATP–DNA complex is shown in Figure 2D, and the ATP-binding site is detailed in Figure 2E. Both monomers of the *HpSoj* dimer equally contribute to DNA-binding, reinforcing the essential function of Soj dimerization. Each monomer binds DNA via the $\alpha 8$, $\alpha 9$ and $\alpha 10$ helices, with the DNA located in a furrow-shaped basic patch formed by four key lysine residues: Lys199 (in $\alpha 8$), Lys227 (in $\alpha 9$), Lys230 (in $\alpha 9$) and Lys247 (in $\alpha 10$) (Figure 3A). Among these DNA-binding residues, Lys227, Lys230 and Lys247 are conserved as either Lys/Arg in the bacterial ParA superfamily, and only Lys247 is threonine in *CcParA* (Supplementary Figure S1). Lys199 reveals sequence diversity as K/I/Q/E in the ParA superfamily (Supplementary Figure S1).

Residues Asn196, Lys199, and Val229 directly interact via hydrogen bonding with phosphate groups of the DNA backbone in the minor groove (Figure 3A). Surprisingly, these DNA-binding residues are not conserved among the ParA superfamily (Supplementary Figure S1). Residues Asn196 and Val229 interact with DNA through the amine nitrogen of the main chain, whereas Lys199 interacts with it via the amine group of the side chain. These interactions between Soj protein and nsDNA in the minor groove are a common feature shared with other nsDNA-binding proteins (50,51). Furthermore, the continuous basic patch created by Lys199, Lys227, Lys230 and Lys247 in the *HpSoj* dimer is required for nsDNA-binding. Our sequence alignment (Supplementary Figure S1) reveals that these basic residues are partially conserved as either Lys/Arg in the bacterial ParA superfamily, so a continuous basic patch might be necessary for nsDNA binding.

The crystal structure of the *HpSoj*–ADP–DNA complex was determined at a resolution of 2.5 Å. The ADP was located in the nucleotide binding site according to the $F_o - F_c$ omit map at 3.0 sigma (Figure 2F). Although ATP had been added in the crystallization setup, the hydrolyzed ADP was observed in the crystal (Figure 2F). Two *HpSoj*–ADP dimers were bound to one DNA molecule, similar to the structure of the *HpSoj*–ATP–DNA complex (Supplementary Figure S3A). The overall structures and ATP-binding sites of the *HpSoj*–ATP–DNA and *HpSoj*–ADP–DNA complexes are similar to those of *HpSoj* (Figure 2C, E, F and Supplementary Figure S3). Based on structural comparison, the root mean square deviation (r.m.s.d.) between the *HpSoj*–ATP and *HpSoj*–ATP–DNA complexes is 0.48 Å (in $C\alpha$), between *HpSoj*–ATP and *HpSoj*–ADP–DNA it is 0.51 Å (in $C\alpha$), and between *HpSoj*–ATP–DNA and *HpSoj*–ADP–DNA it is 0.35 Å (in $C\alpha$). Previous study has shown that the average r.m.s.d. for proteins recognizing nsDNA is <1.0 Å between unbound- and bound-DNA conformations (52). The overall B-factors of *HpSoj*–ADP–DNA and *HpSoj*–ATP–DNA are 59 and 85 Å², respectively (Table 1). The observation that both *HpSoj*–ADP–DNA and *HpSoj*–ATP–DNA share similar structures may be due to ATP hydrolysis during crystallization, which could pre-

vent any subsequent conformational change that might occur in the ADP-bound form.

Structural differences among *HpSoj* and its DNA complexes

Structural comparison of *HpSoj*–ATP and its DNA complexes (Figure 3D) revealed that they share a similar overall structure, with r.m.s.d. values less than 1 Å. PyMOL (53) calculations revealed that helix $\alpha 7$ rotates 5.1° and participates in dimer interactions via residues Glu161/Leu165 (Supplementary Table S2), and that loop $\beta 6\alpha 7$ is involved in ATP binding through residues Glu156/Phe157/Phe158 (Figure 2C and E). Also, we found that helix $\alpha 9$ rotates 4.6° and is involved in DNA binding (Figure 3B), and that loop $\alpha 8\alpha 9$ is involved in ATP binding (Figure 3B). The dimer interfaces of the *HpSoj*–ATP, *HpSoj*–ATP–DNA and *HpSoj*–ADP–DNA complexes are 1440, 1349, and 1313 Å², respectively, based on PISA calculation (48). Given the disparity in interface area between DNA-unbound and -bound *HpSoj* dimer, the monomer-monomer relationship may have to be adjusted in order to interact properly with DNA. Our PyMOL calculations (53) revealed a difference of 3.6° in the angle between $\alpha 4$ of the dimer for *HpSoj*–ATP and *HpSoj*–ATP–DNA. Several hydrogen bonds present in the *HpSoj*–ATP dimer interaction were absent in the *HpSoj*–ATP–DNA complex, all of which were located in $\alpha 2$ and $\alpha 7$ including the hydrogen bonds of Gln43–Gln11 and Ser48–Glu161 (Supplementary Table S2).

Non-specific DNA binding

Protein can non-specifically bind with DNA using positively-charged and surface-exposed residues to interact with the negatively-charged phosphate of the DNA backbone (17). *HpSoj* dimer binds DNA through a continuous basic binding patch formed by Lys199, Lys227, Lys230 and Lys247. Based on the sequence alignment and the structural comparisons, the four corresponding basic residues in *TiSoj* are Arg182/Arg194/Arg208/Arg211, in *BsSoj* they are Arg189/Lys201/Arg215/Arg218, and in *SpParA* they are Lys230/Arg253/Lys256/Lys273 (Supplementary Figure S1). Mutagenesis of *BsSoj* revealed that Arg189 and Arg218 are involved in DNA-binding and mediate the interaction between *BsSoj* and the nucleoid (17). In *SpParA*, Lys256A and Lys273/274A mutation abrogated DNA-binding ability (10,54). Thus, the continuous basic patch may be important for DNA-binding among the bacterial ParA superfamily.

Based on our *HpSoj*–ATP–DNA complex structure, *HpSoj* dimer binds nsDNA through a continuous basic binding patch formed by residues Lys199, Lys227, Lys230, Lys247, as well as Asn196, and Val229 (Figure 3A). Lys199/Asn196 and Lys230/Val229 interact with DNA by clamping the minor groove. Asn196 and Lys199 from $\alpha 8$ exhibit low sequence homology among bacterial ParA (Supplementary Figure S1). Asn196 interacts with DNA through the amine nitrogen of the main chain, whereas Lys199 interacts with DNA via the amine group of the side chain. Val229 and Lys230 of $\alpha 9$ are conserved among bacterial ParA (²²⁹V-K/R-L/V-A/S-E²³³) (Supplementary Figure S1). Val229 interacts with DNA through the amine ni-

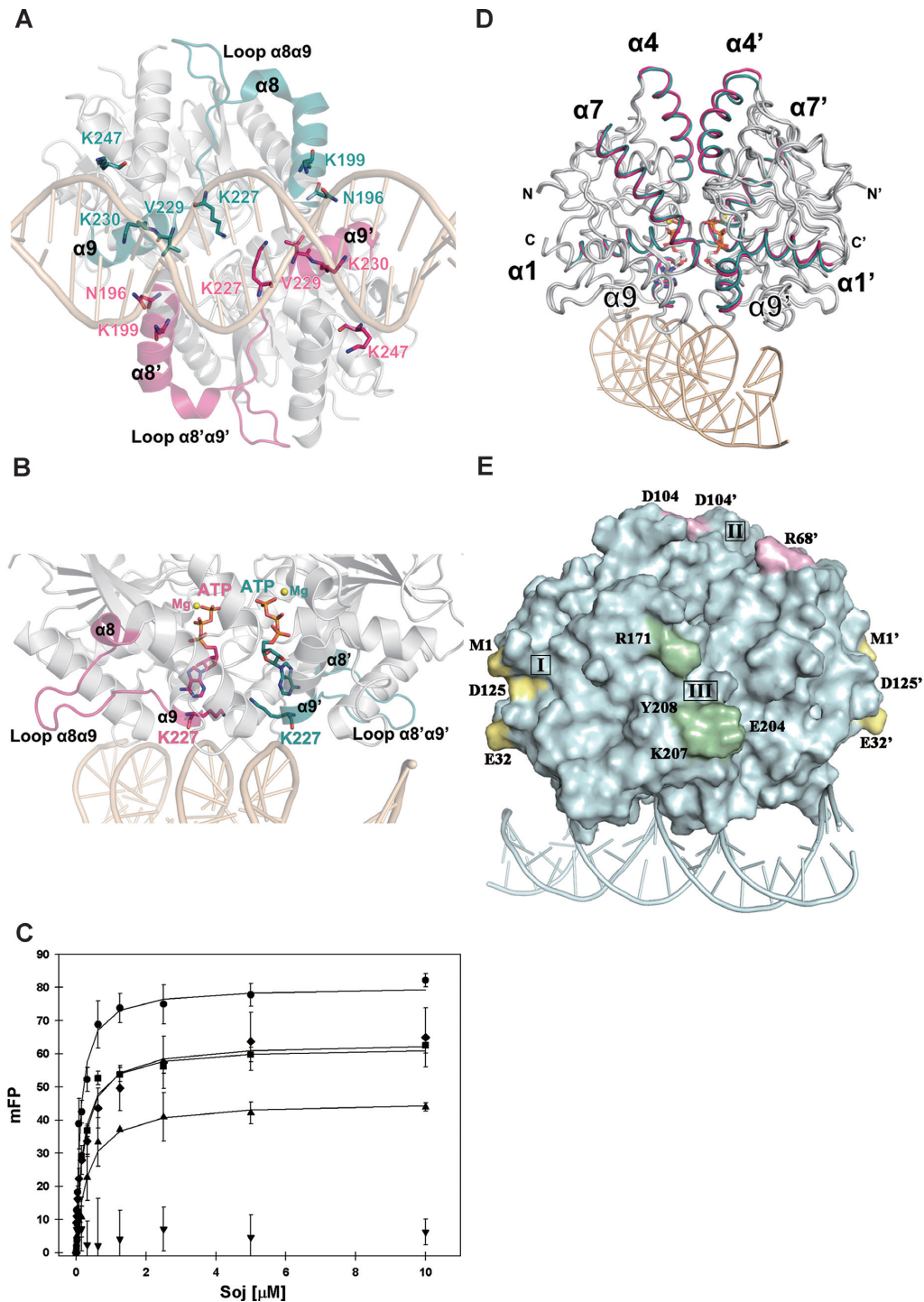


Figure 3. The *HpSoj*-ATP-DNA complex. (A) The detailed interactions between *HpSoj* dimer and DNA of the *HpSoj*-ATP-DNA complex. A close-up view of the interactions between *HpSoj* and DNA related to Figure 2d is shown. The residues of the DNA binding environment (N196, K199, K227, V229, K230, and K247) are shown as sticks. The $\alpha 8$, $\alpha 9$, and loop $\alpha 8\alpha 9$ features that constitute the minor groove clamp of each monomer of the dimer are colored pink and cyan, respectively. (B) The correlated positions of K227, ATP, and DNA of the *HpSoj*-ATP-DNA complex. Loop $\alpha 8\alpha 9$ and K227 from each monomer of the dimer are colored pink and cyan, respectively. (C) The equilibrium DNA binding assays of *HpSoj* and its mutant proteins with *parS24* DNA were done by fluorescence polarization binding isotherms (FP). The *parS24* binding for *HpSoj* (\bullet), *HpSoj*K199E (\blacksquare), *HpSoj*K230E (\blacklozenge), *HpSoj* K199/230E (\blacktriangle) and *HpSoj*K199/227/230/247E (\blacktriangledown) were shown. The corresponding K_d are 122 ± 14 nM ($R^2 = 0.99$), 215 ± 24 nM ($R^2 = 0.99$), 187 ± 36 nM ($R^2 = 0.96$), 308 ± 40 nM ($R^2 = 0.98$) and NB (no measurable binding), respectively. DNA binding was measured by fluorescence polarization (in mFP units), plotted against protein concentration (0–10 μM). The average of three independent experiments is shown with error bars representing one standard deviation of the mean. (D) Superimposition of the *HpSoj*-ATP and *HpSoj*-ATP-DNA structures. The α -helices $\alpha 1$, $\alpha 4$, $\alpha 7$ and $\alpha 9$ of *HpSoj*-ATP and *HpSoj*-ATP-DNA are colored pink and cyan, respectively. (E) Dimer-dimer interaction regions of the *HpSoj*-DNA complex. Three regions participating in the dimer-dimer interface are labeled I, II and III and colored in yellow, pink, and green, respectively. Residues involved in the dimer-dimer interactions are labeled.

trogen of the main chain, but Lys230 does not directly interact with DNA. Lys199 and Lys230 promote DNA binding by inducing their neighboring residues, Asn196 and Val229 respectively, to form hydrogen bonds via their main chains with DNA in the center of the DNA minor groove (Figure 3A). Loop $\alpha 8\alpha 9$ exhibits sequence consensus among bacterial ParA (²²⁴M/V-I-P-K/R-S/N²²⁸) (Supplementary Figure S1). Pro226 and Ser228 directly interact with the adenosine of ATP through their main chains (Figure 2C and Supplementary Table S1). These loop $\alpha 8\alpha 9$ interactions with ATP have also been observed in *Ti*Soj (corresponding to residues Pro207/Arg208/Asn209) (7) and *Sp*ParA (corresponding to residues Lys252/Arg253/Ser254) (10).

Lys227 is highly conserved in the ParA superfamily (Supplementary Figure S1). Interestingly, Lys227 is located at the core of the DNA binding surface, but its side chain is oriented away from the DNA and it does not directly interact with DNA (Figure 3A). Moreover, this residue is embedded inside the dimer interface and interacts with the ribose of ATP through a water molecule (Figure 2C and Supplementary Table S1). Thus, significantly, Lys227 might play an important role in linking ATP- and DNA-binding in the *Hp*Soj dimer (Figure 3B). The orientation of the Lys227 side chain is important for adjusting loop $\alpha 8\alpha 9$ to interact with ATP. In the presence of DNA, Lys227 is located at the core of the *Hp*Soj DNA-binding surface, at a distance of 4.3–7.2 Å from the DNA molecule. In addition, Lys247 exhibits sequence homology among the bacterial ParA superfamily (except for *Ti*Soj: Thr228) (Supplementary Figure S1), and is located 4.9–8.0 Å from DNA, so it might play an interactive role in the DNA binding of bacterial ParA. Thus, based on our analyses of these residues, $\alpha 8$, loop $\alpha 8\alpha 9$ and $\alpha 9$ are important functional regions for ATP- and DNA-binding and they link these two functions in the ParA superfamily.

Based on the crystal structure of the *Hp*Soj-ATP-DNA complex (Figure 3A), four key lysine residues (Lys199, Lys227, Lys230 and Lys247) are involved in the non-specific DNA binding. The *Hp*Soj mutants, K199E, K230E, K199/230E and K199/227/230/247E, have been isolated and purified. Meanwhile, their non-specific DNA binding were measured by the fluorescence polarization (FP) and shown in Figure 3C. The K_d of non-specific DNA binding of wildtype *Hp*Soj is calculated to be 122 nM. However, the non-specific DNA binding of the mutants are decreased and the K_d for K199E, K230E and K199/230E are 187, 215, 308 nM, respectively. Nevertheless, the K_d of mutant K199/230/230/247E is undetectable. Indeed, it suggested that Lys199, Lys227, Lys230 and Lys247 play an important role in the non-specific DNA binding of *Hp*Soj.

Protein-protein interactions of *Hp*Soj-DNA complexes

We observed *Hp*Soj dimer-dimer interactions at several locations, but the DNA-binding region is preserved in the DNA-unbound state (Figure 3E). Dimer-dimer interactions were observed in three regions of *Hp*Soj-DNA complexes (I, II and III in Figure 3E). The buried surface areas of these regions were calculated for *Hp*Soj-ATP-DNA and *Hp*Soj-ADP-DNA as 295 and 319 Å² (region I), 392 and 558 Å² (region II), and 317 and 305 Å² (region III), re-

spectively. Among the three interfaces, region II contributes most to protein-protein interactions. Region II is mainly formed by helix $\alpha 4$ that displays diverse sequence and length among the ParA superfamily (Supplementary Figure S1). The calculated buried surface area of region II is 488 Å² for *Hp*Soj-ATP alone. After DNA binding, *Hp*Soj-ATP-DNA adopts an active state with fewer protein-protein interactions. *Hp*Soj-ADP-DNA may adopt a relaxed state and return to the DNA-unbound state, so it has a similar protein-protein interaction area as that of *Hp*Soj-ATP.

Superimposition of *Hp*Soj-ATP and the *Hp*Soj-ATP-DNA complexes relative to the AB dimer (Supplementary Figure S3B) revealed an ~9–10 Å deviation between the CD dimers (C α of Thr98 in $\alpha 4$, and C α of Lys207 in $\alpha 8$). After DNA binding, dimer-dimer interactions affect the relationship of the AB and CD dimers to induce a molecular shift in the CD dimer (Supplementary Figure S3B). Although the *Hp*Soj dimer only has one DNA-binding site, it possesses numerous dimer-dimer interaction regions to recruit *Hp*Soj molecules (Figure 3E and Supplementary Figure S3B).

The protein-protein interactions of *Hp*Soj dimer might play an essential role in facilitating *Hp*Soj localization to high-density DNA regions (HDRs, Supplementary Figure S4A) in the *H. pylori* ParABS system. It has previously been reported that the DNA-binding activity of ParA is essential for localization of all components of the partitioning machinery to HDRs and for a stable HDR-bound ParA state (32). Accordingly, the *Hp*Soj-ATP-DNA structure might mimic the stable and active HDR-bound state (Supplementary Figure S4A). In the multifaceted DNA-binding site of pNOB8 ParA-DNA, each ParA dimer is surrounded by a dense DNA substrate (Supplementary Figure S4B) (37). The sole DNA-binding site in our *Hp*Soj-DNA complex structure (Figure 3E), *Hp*Soj dimers can be recruited by protein-protein interactions to engage several DNA substrates (Supplementary Figure S4A).

Structural comparison between *Hp*Soj and pNOB8 ParA

We superimposed the structures of *Hp*Soj and pNOB8 ParA monomers and found an r.m.s.d. of 5.5 Å (C α atom), with conformational differences at $\alpha 4$ and loop $\alpha 8\alpha 9$, as well as several insertions in $\alpha 8$, $\alpha 9$, $\alpha 10$, loop $\alpha 2\alpha 3$, loop $\beta 3\beta 4$, loop $\alpha 7\beta 7$ and loop $\alpha 10\alpha 11$ of pNOB8 ParA (Figure 4A). However, *Hp*Soj and pNOB8 ParA share a similar ATP-binding site. The dimer interfaces of *Hp*Soj-ATP and the *Hp*Soj-ATP-DNA complex are 1440 and 1349 Å², respectively, whereas they are 1861 and 1849 Å² for pNOB8 ParA and pNOB8 ParA-AMPPNP-DNA. Moreover, the *Hp*Soj and pNOB8 ParA dimers are dissimilar and the relationships between their monomers are different (Figure 4B).

In the *Hp*Soj-DNA complex, the continuous basic patch of *Hp*Soj is exposed for DNA binding (Figure 4D). The pNOB8 ParA and its DNA complex reveal a different dimer conformation (35,37). The corresponding DNA-binding residues of *Hp*Soj (Asn196, Lys199, Lys227, Val229, Lys230, Lys247) in pNOB8 are Arg210/Ala214/Arg257/Lys258/Glu259/Val288, but Arg257/Lys258/Glu259/Val288 are missing from the crystal structure of the ParA-AMPPNP-DNA complex (PDB ID: 5U1J). In the pNOB8 ParA-AMPPNP-DNA complex,

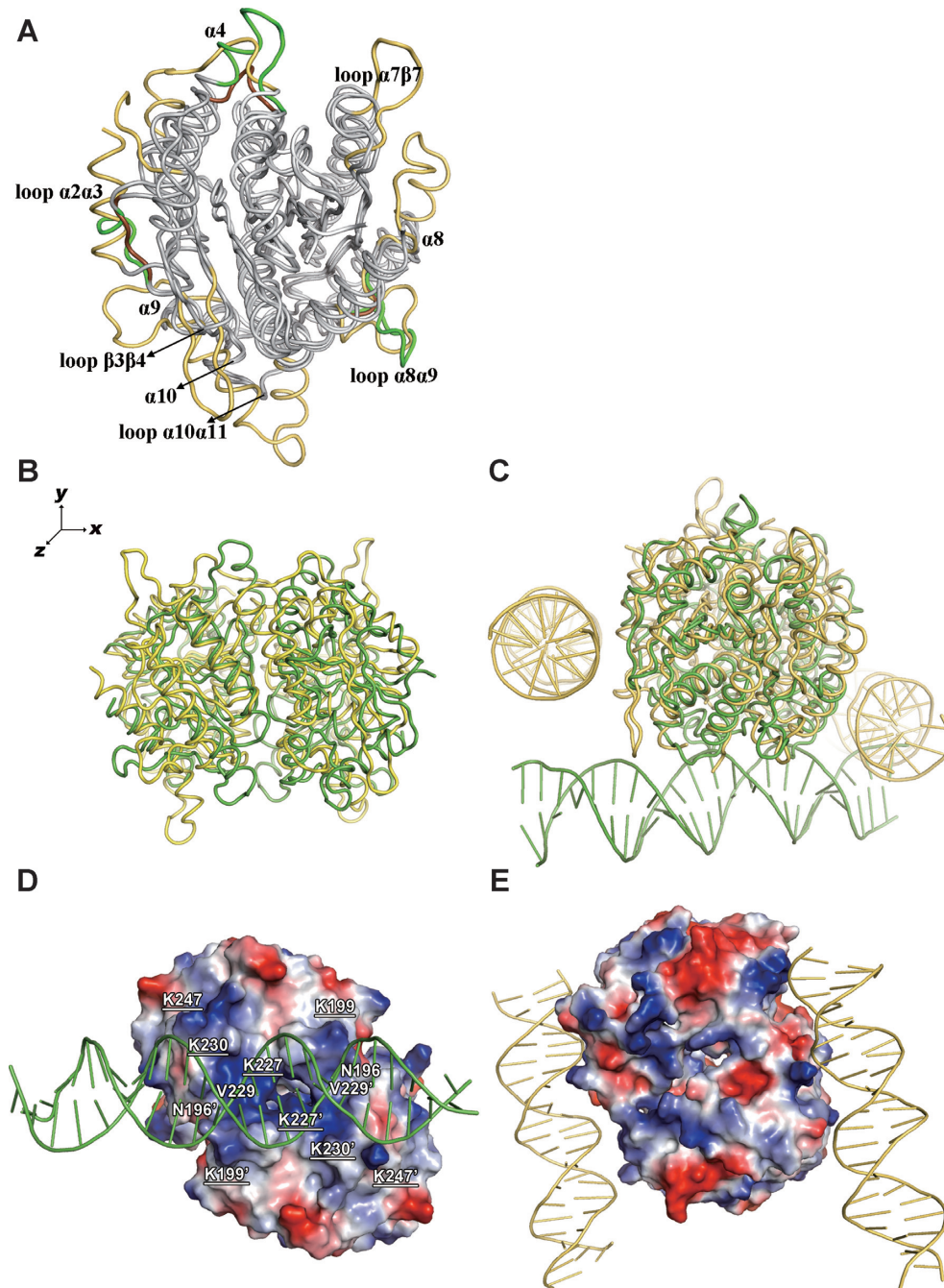


Figure 4. *HpSoj* and pNOB8 ParA. (A) Superimposition of the *HpSoj*, *TtSoj*, and pNOB8 ParA monomers. The main structural differences are labeled as loop $\alpha 2\alpha 3$, $\alpha 4$, and loop $\alpha 8\alpha 9$, which are colored green, brown and yellow for *HpSoj*, *TtSoj*, and pNOB8 ParA, respectively. (B) Structural superimposition of the *HpSoj* and pNOB8 ParA dimers. The *HpSoj* and pNOB8 ParA dimers are colored green and yellow, respectively. (C) Structural superimposition of the *HpSoj*-DNA and pNOB8 ParA-DNA dimers. The orientation of *HpSoj*-DNA is rotated 90° along the y -axis of that complex in (B). *HpSoj* and pNOB8 ParA are colored as shown in (B) and their bound DNAs are shown as ribbons and colored accordingly. (D) Electrostatic surface representation of the *HpSoj*-DNA complex. Positive and negative potentials are shown in blue and red, respectively. The orientation of the *HpSoj*-DNA complex is rotated 90° along the x -axis relative to that in (B). Residues involved in DNA-binding from each monomer of the dimer are labeled. Residues Lys199, Lys227, Lys230 and Lys247 that form the basic-patch for DNA binding are labeled and underlined. (E) Electrostatic surface representation of the pNOB8 ParA-DNA complex. Positive and negative potentials are shown in blue and red, respectively. The orientation of the pNOB8 ParA-DNA complex is rotated 90° along the x -axis relative to that in (C).

the two monomers of the ParA dimer need to be rotated to expose basic residues (Arg52, Lys58, Lys85, Lys218, Lys221 and Lys 270) for optimal DNA binding. *HpSoj* region III (responsible for dimer-dimer interactions; Figures 3E and 4C) corresponds to the DNA-binding residues of pNOB8 ParA. Notably, the electrostatic surface distribution of the DNA-binding region of *HpSoj* is predominantly basic, whereas it is evenly distributed among basic/acidic in the pNOB8 ParA–AMPPNP–DNA complex (PDB ID: 5K5Z) (Figure 4D and E).

The bacterial and archaeal partitioning system

The partitioning system in most bacteria involves two proteins (ParA and ParB) and a *cis*-acting centromere-like *parS* DNA (55). Two partitioning systems have been described in archaea; the SegAB system and AspA–ParBA that comprise different key functional proteins (36). We superimposed the monomer structures of *HpSoj* and *TtSoj* (Figure 4A) and found that they share a similar overall structure, with an r.m.s.d. of 0.8 Å (C α atom). Structural differences between the *HpSoj* and *TtSoj* monomers mainly occur in α 4 and loops α 2 α 3 and α 8 α 9 (Figure 4A). Loop α 2 α 3 and α 4 are involved in dimer-dimer interactions (Supplementary Table S2), and loop α 8 α 9 participates in ATP-binding (Supplementary Table S1). *HpSoj* has longer α 4 (residues 99–111) and loop α 8 α 9 (residues 211–224) regions than *TtSoj* (Supplementary Figure S1). However, the dimer relationships of both *HpSoj* and *TtSoj* are quite similar (Figure 5A and B). Based on the crystal structure of the *HpSoj*–ATP–DNA complex, we postulate a possible DNA-binding patch in *TtSoj* created by residues Arg182, Arg208, Arg211 and Thr228 (Figure 5B). Significantly, a basic patch can also be observed for *SpParA* (Lys230, Arg253, Lys256 and Lys273) (Figure 5C) and for TP228 ParA (Asn148, Arg169, Lys174 and Lys191) (Figure 5D), which also correspond to the DNA-binding basic patch of *HpSoj*. These findings suggest that bacterial ParA superfamily might have a similar nsDNA-binding mode as that *HpSoj* has.

In the archaeal SegAB system, the ATPase SegA is polymerized upon binding ATP, and the site-specific DNA-binding protein SegB promotes SegA polymerization (34). In the archaeal AspA–ParBA machinery, pNOB8 ParA–AMPPNP forms a polymer in the absence of DNA but not in the presence of DNA (37). *HpSoj* does not form a polymer, regardless of the presence of nucleotide or DNA. *HpSoj* and pNOB8 ParA reveals different monomer relationships of their dimers (Figure 4B). Remarkably, there is a significant discrepancy in DNA binding between *HpSoj* and pNOB8 ParA (Figure 4C); *HpSoj* dimer binds one DNA at the base of the molecule, whereas the pNOB8 ParA dimer binds two DNA molecules at two sides of the molecule (Figure 4C). *HpSoj* and pNOB8 ParA also have different DNA-binding surfaces; 504 Å² for the sole DNA-binding site of *HpSoj* and 238 and 194 Å² for the two pNOB8 ParA DNA-binding sites (Figure 4C), as calculated by PISA (48). The solvent content of the *HpSoj*–ATP–DNA and pNOB8 ParA–AMPPNP–DNA complexes are 58% and 45%, respectively. The pNOB8 ParA–AMPPNP–DNA complex contains multiple DNA-binding sites and the low solvent content induces tight molecular packing between pNOB8

ParA and the DNA (Supplementary Figure S4B). Thus, structural comparison of *HpSoj*–ATP–DNA and pNOB8 ParA–AMPPNP–DNA complexes demonstrates that the mode of nsDNA-binding might differ between bacteria and archaea. Despite this difference, they might share a similar DNA segregation mechanism to drive movement of the ParB–DNA cargo, which does not require ParA polymerization.

Nucleoid–adaptor complex (NAC) formation

To investigate ParABS nucleoid-adaptor complex (NAC) formation in *H. pylori*, we used EM to directly capture *HpSpo0J* and *HpSoj* in complex with DNA (Figure 6). We used *parS550* for specific DNA-binding by *HpSpo0J* and 180DNA as a substrate for *HpSoj* to probe the *HpSpo0J*–*HpSoj*–DNA complex based on the differing DNA lengths. We assessed [*HpSpo0J*:*parS550*] experiment, a total of 203 conformational complexes were counted, including 70.9% of the single *HpSpo0J*:*parS550* complex (Figure 6A), 12.8% of the *HpSpo0J*:*parS550* paired complex (Figure 6B), and 16.3% of a higher-order complex (Figure 6C) (Table 2). However we observed NAC complex formation when we co-incubated [*HpSpo0J*:*parS550*] (the partitioning complex, cargo) with [*HpSoj*–180DNA] (the nucleoid-bound complex) (Figure 6F–H). We counted a total of 173 conformational complexes in this latter experiment (Table 2), comprising 72.3% of the single *HpSpo0J*:*parS550* complex, 6.9% of the *HpSpo0J*:*parS550* paired complex, 18.5% of the [*HpSpo0J*:*parS550*]+[*HpSoj*:180DNA] complex (i.e. the NAC complex), and 2.3% of a higher-order complex. Thus, significant amounts of NAC complexes were detected when both *HpSoj* and *HpSpo0J* interacted with the assistance of the specific *parS* DNA. It suggests that *HpSoj* and DNA involvements might promote *HpSoj*–*HpSpo0J* interaction to form the NAC complex, instead of making *HpSpo0J*–*HpSpo0J* interaction to form the high order complex.

The [*HpSpo0J*:*parS550*]+[*HpSpo0J*:180DNA] data revealed that DNA with a specific *parS* sequence can facilitate *HpSpo0J*–*HpSpo0J* interaction to form the *HpSpo0J*–DNA paired complex and the higher-order complexes, whereas the DNA without the *parS* site might disrupt formation of these complexes. Also, we used DNA without a *parS* site (600DNA) to examine formation of the *HpSpo0J*–DNA paired complex. *HpSpo0J*:600DNA paired and higher-order complexes accounted for 3.6% and 0.5%, respectively (Supplementary Table S3) (as opposed to 12.8%/16.3% in *HpSpo0J*:*parS550* complexes), suggesting that *parS* DNA is essential for their formation. Moreover, only 2.0% NAC formation was observed for this experiment (Supplementary Table S3) (as opposed to 18.5% for [*HpSpo0J*:*parS550*]+[*HpSoj*:180DNA]), supporting that *parS* DNA promotes NAC formation. Furthermore, inclusion of *HpSoj* disrupted formation of the *HpSpo0J*:600DNA paired complex (from 3.6% to 1.5%).

DISCUSSION

In this study, we determined the ATPase activity of *HpSoj* and found that it is promoted by *HpSpo0J* and DNA-binding. We solved the crystal structures of *HpSoj* and its

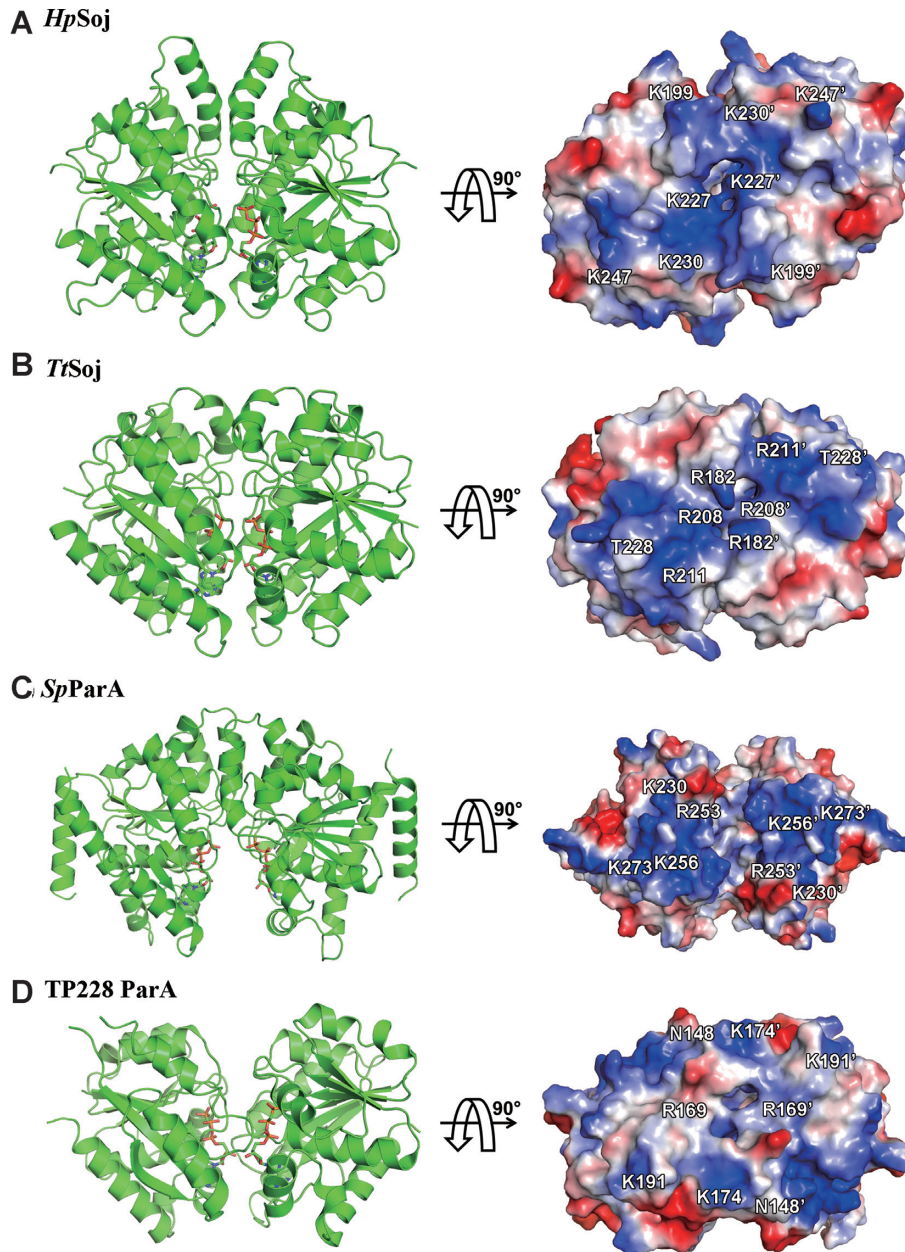


Figure 5. Structural comparison of the bacterial ParA superfamily. Comparison of the electron surface potentials of various bacterial ParA proteins. The *HpSoj*, *TtSoj*, *SpParA* and TP228 ParA dimers are shown as ribbons (left panel), and their electronic surface potentials (right panel) are shown as 90° rotations along the *x*-axis of the view shown in the left panel. Positive and negative potentials are shown in blue and red, respectively.

DNA-bound complexes, *HpSoj*–ATP–DNA and *HpSoj*–ADP–DNA. From our EM data, we observed possible interactions among *HpSoj*, *HpSpo0J*, and DNA and propose potential NAC formation for the *H. pylori* ParABS system.

HpSoj behaves typically as other ParAs revealing a weak ATPase that is stimulated by DNA and *HpSpo0J*/ParB. The ATPase activity of *HpSoj* is stimulated by the *HpSpo0J*–*parS* complex. When *HpSpo0J* binds to *parS55* and the *HpSpo0J*–*parS* complex is formed the *N*-terminal domain of *HpSpo0J* might be exposed based on the crystal structure of the *HpSpo0J*–*parS* complex (2). And then the *N*-terminal domain might interact with *HpSoj* to promote the ATPase activity. In addition, the ATPase activ-

ity of *HpSoj* was stimulated by *HpSpo0JN* in the presence of DNA. Although *HpSpo0JN* does not contain the DNA binding domain it still can stimulate the ATPase activity. This phenomenon also has been reported that the SopB ATPase activation domain exists at its *N*-terminus, which does not have the DNA binding domain either (56). Several previous functional studies demonstrated that the *N*-terminal domain of ParB likely contributes to the ParA/ParB interaction and to promote ParA ATPase activity (7,16,57,58). A weak interaction between *HpSoj* and *HpSpo0JN* was detected by MST and it perhaps due to their dynamic and transient association.

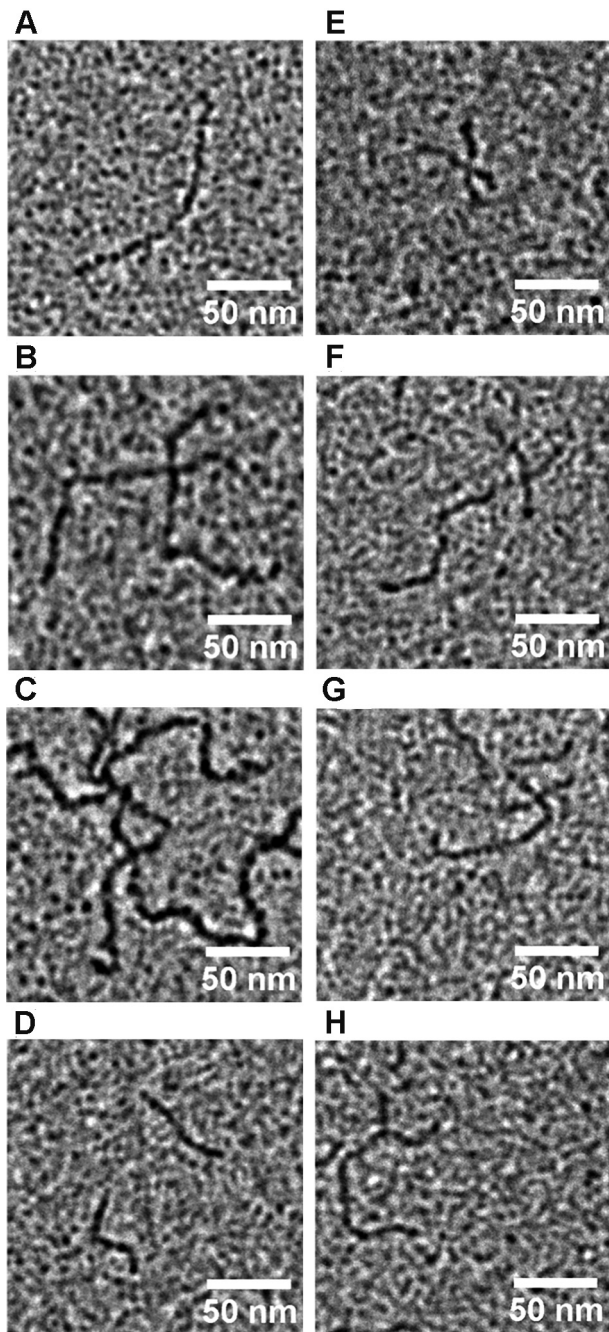


Figure 6. Electron microscopy images of *HpSoj* and *HpSpo0J* nucleoprotein complexes. EM images of *HpSoj*, *HpSpo0J* and DNA complexes. (A) The *HpSpo0J*–*parS550* single complex. (B) The *HpSpo0J*–*parS550* paired complex. (C) The higher-order complex of *HpSpo0J*–*parS550*. (D) The *HpSoj*–180DNA complex. (E) The *HpSoj*–180DNA paired complex. (F), (G) and (H) are images of three different [*HpSpo0J*:*parS550*]+[*HpSoj*:180DNA] complexes.

Single-molecule and 3D structured illumination microscopy studies (17,18,31,32) have indicated that the nsDNA-binding ability of ParA is critical in DNA segregation. The *HpSoj* dimer binds to one DNA molecule, whereas the archaeal *Sulfolobus* pNOB8 ParA dimer binds to two DNA molecules via multifaceted interactions (37)

(Figure 4C). The DNA-binding regions of *HpSoj* and pNOB8 ParA differ, involving different non-conserved residues, perhaps because of species variation or because the DNA-binding of ParA is non-specific. Regarding the electrostatic surface of the ParA dimer, a basic patch environment and a proper binding curvature are required for nsDNA binding.

Previous biochemical studies identified that ParA binds with ATP to form a dimer and then undergoes a slow conformational change into the ‘ParA*₂-ATP₂’ state that is stable and, based on tryptophan fluorescence assays on P1 ParA, precise for DNA binding (26). A continuous and basic DNA-binding patch (comprising residues Lys199, Lys 227, Lys 230 and Lys247) is created when *HpSoj* is dimerized in the ParA*₂-ATP₂ state. However, there is no significant conformational difference between *HpSoj*-ATP and the *HpSoj*-ATP-DNA complex, as is the case for other nsDNA-binding proteins (52). Since the DNA-binding patch is on the *HpSoj* dimer surface and readily exposed for DNA binding, a further conformational change is not necessary. In the absence of ATP, *HpSoj* was not stable and the crystallization was not succeeded. Since the three-dimensional structure of apo-*HpSoj* (no nucleotide) is not available we cannot rule out the possibility of a different conformation among apo-*HpSoj*, *HpSoj*-ATP and *HpSoj*-ATP-DNA. In addition, multiple conformations of *HpSoj*-ATP might exist in solution as that reported in P1 ParA (26).

The pNOB8 ParA, which resembles bacterial ParA, possesses nsDNA-binding ability (37), and a multifaceted DNA-binding mode. The pNOB8 ParB contains an N-terminal domain (residues 1–320) that corresponds to bacterial ParB (182–336 residues), albeit with low sequence homology (35). The pNOB8 ParB binds DNA in a non-specific manner; however, bacterial ParB specifically binds DNA at the *parS* site (35). These Walker-box partitioning systems are ubiquitous and exist in both bacteria (ParABS) and archaea (SegAB and Aspa-ParBA), though each exhibits their own particular mechanisms. In contrast, the DNA-binding patch of pNOB8 ParA is buried inside the dimer so monomer rotation is necessary to expose its basic residues for optimal DNA binding (37). Residues Lys199, Lys 227, Lys 230 and Lys247 form the basic DNA-binding patch of *HpSoj*, with the corresponding residues in pNOB8 ParA being Ala214, Glu250, Ile253 and Lys270. The *HpSoj* basic residues form a DNA-binding patch that harbors one DNA molecule, whereas the dispersed pNOB8 ParA basic residues result in a multifaceted DNA-binding surface, together suggesting that the DNA-binding mechanism of bacterial ParA is significantly different from that of archaeal ParA.

The *HpSoj*-ADP-DNA complex presented a similar conformation to that of *HpSoj*-ATP-DNA. Thus, the *HpSoj*-ADP-DNA complex might represent a transitional state in which the ATP has been hydrolyzed to ADP but the DNA remains bound. Interaction of *HpSoj* with *HpSpo0J* stimulates ATPase activity (Figure 1A) and may accelerate dimer dissociation and DNA release. In *Salmonella newport* TP228, ParB interacts with the dimer interface of ParA, which may induce ParA to dissociate from DNA, resulting in segregation along the nucleoid matrix (37).

HpSoj does not form a nucleoprotein filament based on our EM data. Also, the hypothesis of ParA polymerization has been excluded with biochemical data and super-resolution microscopy (26,27,29–32). *HpSoj* may be similar to all ParAs that follow the diffusion-ratchet mechanism whereby the ParB partitioning cargo moves on the nucleoid through the chemical gradient of ParA. However, structural results show that the architectures of the DNA segregation systems in bacteria and archaea exhibit two distinct differences: (i) bacterial ParA have only one nsDNA-binding site, but archaeal ParA have two; and (ii) bacterial ParB specifically use the *N*-terminus for ParA interaction (7,35,56,57,59–61), whereas archaeal ParB utilizes a flexible linker to interact with ParA (35). Moreover, ParB in archaeal AspA-ParBA systems does not possess specific DNA-binding ability, which instead is carried out by another protein, AspA (35).

Despite significant differences in the sequence homology, in the manner of DNA binding, and in the three-dimensional structures of ParA protein, both bacteria and archaea modulate DNA segregation that does not require ParA polymerization. The ParA/ParB complex may undergo dynamic and transient conformational change to control the movement of the ParB-DNA cargos (28,29). Interaction between ParA and ParB is known to be weak (6,26), as we observed from our MST assay on *HpSoj* and *HpSpo0JN* (Figure 1B).

Previous EM analysis revealed ParB-mediated centromere pairing in *E. coli* (20), with both paired and higher-order (36%) complexes forming at low ParB concentrations, whereas mostly higher-order complexes were formed at high ParB concentrations. That study concluded that ParB mediated centromere pairing through its *N*-terminal end. The crystal structure of the *HpSpo0J* and *parS* complex in *H. pylori* (2) is an elongated structure, with a flexible *N*-terminal domain for protein-protein interaction and a conserved DNA-binding domain for *parS* binding. *HpSpo0J* interacts vertically and horizontally with its neighbors through the *N*-terminal domain to form an oligomer by adjacent and transverse interactions that might be necessary for molecular assembly of a higher-order nucleoprotein complex (2).

Our EM results (Figure 6 and Table 2 and Supplementary Table S3) show that the *HpSpo0J*/ParB paired complex was significantly reduced when the DNA substrated lacked a *parS* site (600DNA) and when *HpSoj*/ParA ([*HpSoj*:180DNA]) was included. Thus, the *parS* site might regulate the *HpSpo0J*/ParB pairing interaction. In contrast, participation of *HpSoj*/ParA promotes the *HpSoj*-*HpSpo0J* (ParA-ParB) interaction to make the *HpSpo0J*-*HpSoj*-DNA complex with the assistance of the *parS* site. In summary, NAC complex formation could be promoted through *HpSoj* participation and the assistance of specific *parS* site DNA. In *E. coli* P1 ParABS, protein-DNA binding by the ParA-ParB-DNA complex occurs through both specific and non-specific DNA binding by ParB and ParA, respectively, and *parS* site stabilizes this nucleoprotein complex formation (22). Similarly, the NAC is created by interaction of plasmid-bound ParB and nucleoid-bound ParA (32). The DNA replication in *H. pylori*, the ParB paired complex was formed to condense the DNA. When the ParB paired complex encounters ParA, this complex may be de-

stroyed by the ParA and ParB interactions that may promote the NAC formation to carry out DNA segregation.

DATA AVAILABILITY

The atomic coordinates and structure factors have been deposited in the Protein Data Bank (<http://www.rcsb.org/pdb>) with PDB ID codes 6IUB (*HpSoj*-ATP), 6IUD (*HpSoj*-ADP-DNA) and 6IUC (*HpSoj*-ATP-DNA).

SUPPLEMENTARY DATA

Supplementary Data are available at NAR Online.

ACKNOWLEDGEMENTS

We thank the National Synchrotron Radiation Research Center (NSRRC) for access to beam line TPS05A and TLS15A and Spring-8 for access to beam line 44XU and the in-house X-ray facility in the Macromolecular X-ray Crystallographic Center of National Tsing Hua University. We thank the Image Core Facility at the Institute of Molecular Biology, Academia Sinica for electron microscopy.

FUNDING

Ministry of Science and Technology, Taiwan [104-2311-B-007-006-MY3, 105-2627-M-007-005-, 106-2311-B-007-007-MY3 and 107-2321-B-007-004- to Y.-J.S., 104-2311-B-001-016-MY3 to C.-D.H.]; Program for Translational Innovation of Biopharmaceutical Development-Technology Supporting Platform Axis [107-0210-01-19-04]. Funding for open access charge: Ministry of Science and Technology, Taiwan.

Conflict of interest statement. None declared.

REFERENCES

1. Reyes-Lamothe, R., Nicolas, E. and Sherratt, D.J. (2012) Chromosome replication and segregation in bacteria. *Annu. Rev. Genet.*, **46**, 121–143.
2. Chen, B.W., Lin, M.H., Chu, C.H., Hsu, C.E. and Sun, Y.J. (2015) Insights into ParB spreading from the complex structure of Spo0J and parS. *PNAS*, **112**, 6613–6618.
3. Salje, J., Gayathri, P. and Lowe, J. (2010) The ParMRC system: molecular mechanisms of plasmid segregation by actin-like filaments. *Nat. Rev. Microbiol.*, **8**, 683–692.
4. Tran, N.T., Stevenson, C.E., Som, N.F., Thanapipatsiri, A., Jalal, Adam S B. and Le, Tung B K. (2018) Permissive zones for the centromere-binding protein ParB on the *Caulobacter crescentus* chromosome. *Nucleic Acids Res.*, **46**, 1196–1209.
5. Graham, T.G., Wang, X., Song, D., Etson, C.M., van Oijen, A.M., Rudner, D.Z. and Loparo, J.J. (2014) ParB spreading requires DNA bridging. *Genes Dev.*, **28**, 1228–1238.
6. Volante, A. and Alonso, J.C. (2015) Molecular anatomy of ParA-ParA and ParA-ParB interactions during plasmid partitioning. *J. Biol. Chem.*, **290**, 18782–18795.
7. Leonard, T.A., Butler, P.J. and Lowe, J. (2005) Bacterial chromosome segregation: structure and DNA binding of the Soj dimer—a conserved biological switch. *EMBO J.*, **24**, 270–282.
8. Schumacher, M.A. (2012) Bacterial plasmid partition machinery: a minimalist approach to survival. *Curr. Opin. Struct. Biol.*, **22**, 72–79.
9. Dunham, T.D., Xu, W., Funnell, B.E. and Schumacher, M.A. (2009) Structural basis for ADP-mediated transcriptional regulation by P1 and P7 ParA. *EMBO J.*, **28**, 1792–1802.

10. Pratto, F., Cicek, A., Weihofen, W.A., Lurz, R., Saenger, W. and Alonso, J.C. (2008) Streptococcus pyogenes pSM19035 requires dynamic assembly of ATP-bound ParA and ParB on parS DNA during plasmid segregation. *Nucleic Acids Res.*, **36**, 3676–3689.
11. Schumacher, M.A., Ye, Q., Barge, M.T., Zampini, M., Barilla, D. and Hayes, F. (2012) Structural mechanism of ATP-induced polymerization of the partition factor ParF: implications for DNA segregation. *J. Biol. Chem.*, **287**, 26146–26154.
12. McLeod, B.N., Allison-Gamble, G.E., Barge, M.T., Tonthat, N.K., Schumacher, M.A., Hayes, F. and Barilla, D. (2017) A three-dimensional ParF meshwork assembles through the nucleoid to mediate plasmid segregation. *Nucleic Acids Res.*, **45**, 3158–3171.
13. Lee, M.J., Liu, C.H., Wang, S.Y., Huang, C.T. and Huang, H. (2006) Characterization of the Soj/Spo0J chromosome segregation proteins and identification of putative parS sequences in *Helicobacter pylori*. *Biochem. Biophys. Res. Commun.*, **342**, 744–750.
14. Oliva, M.A. (2016) Segrosome complex formation during DNA trafficking in bacterial cell division. *Front. Mol. Biosci.*, **3**, 51.
15. Baxter, J.C. and Funnell, B.E. (2014) Plasmid partition mechanisms. *Microbiol. Spectr.*, **2**, PLAS-0023-2014.
16. Scholefield, G., Whiting, R., Errington, J. and Murray, H. (2011) Spo0J regulates the oligomeric state of Soj to trigger its switch from an activator to an inhibitor of DNA replication initiation. *Mol. Microbiol.*, **79**, 1089–1100.
17. Hester, C.M. and Lutkenhaus, J. (2007) Soj (ParA) DNA binding is mediated by conserved arginines and is essential for plasmid segregation. *PNAS*, **104**, 20326–20331.
18. Castaing, J.P., Bouet, J.Y. and Lane, D. (2008) F plasmid partition depends on interaction of SopA with non-specific DNA. *Mol. Microbiol.*, **70**, 1000–1011.
19. Jensen, R.B., Lurz, R. and Gerdes, K. (1998) Mechanism of DNA segregation in prokaryotes: replicon pairing by parC of plasmid R1. *PNAS*, **95**, 8550–8555.
20. Ringgaard, S., Lowe, J. and Gerdes, K. (2007) Centromere pairing by a plasmid-encoded type I ParB protein. *J. Biol. Chem.*, **282**, 28216–28225.
21. Edgar, R., Chattoraj, D.K. and Yarmolinsky, M. (2001) Pairing of P1 plasmid partition sites by ParB. *Mol. Microbiol.*, **42**, 1363–1370.
22. Havey, J.C., Vecchiarelli, A.G. and Funnell, B.E. (2012) ATP-regulated interactions between P1 ParA, ParB and non-specific DNA that are stabilized by the plasmid partition site, parS. *Nucleic Acids Res.*, **40**, 801–812.
23. Bouet, J.Y. and Funnell, B.E. (1999) P1 ParA interacts with the P1 partition complex at parS and an ATP-ADP switch controls ParA activities. *EMBO J.*, **18**, 1415–1424.
24. Ringgaard, S., van Zon, J., Howard, M. and Gerdes, K. (2009) Movement and equipositioning of plasmids by ParA filament disassembly. *PNAS*, **106**, 19369–19374.
25. Ptacin, J.L., Lee, S.F., Garner, E.C., Toro, E., Eckart, M., Comolli, L.R., Moerner, W.E. and Shapiro, L. (2010) A spindle-like apparatus guides bacterial chromosome segregation. *Nat. Cell Biol.*, **12**, 791–798.
26. Vecchiarelli, A.G., Han, Y.W., Tan, X., Mizuuchi, M., Ghirlando, R., Biertumpfel, C., Funnell, B.E. and Mizuuchi, K. (2010) ATP control of dynamic P1 ParA-DNA interactions: a key role for the nucleoid in plasmid partition. *Mol. Microbiol.*, **78**, 78–91.
27. Vecchiarelli, A.G., Mizuuchi, K. and Funnell, B.E. (2012) Surfing biological surfaces: exploiting the nucleoid for partition and transport in bacteria. *Mol. Microbiol.*, **86**, 513–523.
28. Vecchiarelli, A.G., Neuman, K.C. and Mizuuchi, K. (2014) A propagating ATPase gradient drives transport of surface-confined cellular cargo. *PNAS*, **111**, 4880–4885.
29. Hwang, L.C., Vecchiarelli, A.G., Han, Y.W., Mizuuchi, M., Harada, Y., Funnell, B.E. and Mizuuchi, K. (2013) ParA-mediated plasmid partition driven by protein pattern self-organization. *EMBO J.*, **32**, 1238–1249.
30. Lim, H.C., Surovtsev, I.V., Beltran, B.G., Huang, F., Bewersdorf, J. and Jacobs-Wagner, C. (2014) Evidence for a DNA-relay mechanism in ParABS-mediated chromosome segregation. *Elife*, **3**, e02758.
31. Surovtsev, I.V., Campos, M. and Jacobs-Wagner, C. (2016) DNA-relay mechanism is sufficient to explain ParA-dependent intracellular transport and patterning of single and multiple cargos. *PNAS*, **113**, E7268–E7276.
32. Le Gall, A., Cattoni, D.I., Guilhas, B., Mathieu-Demaziere, C., Oudjedi, L., Fiche, J.B., Rech, J., Abrahamsson, S., Murray, H., Bouet, J.Y. et al. (2016) Bacterial partition complexes segregate within the volume of the nucleoid. *Nat. Commun.*, **7**, 12107.
33. Gerdes, K., Moller-Jensen, J. and Bugge Jensen, R. (2000) Plasmid and chromosome partitioning: surprises from phylogeny. *Mol. Microbiol.*, **37**, 455–466.
34. Kalliomaa-Sanford, A.K., Rodriguez-Castañeda, F.A., McLeod, B.N., Latorre-Roselló, V., Smith, J.H., Reimann, J., Albers, S.V. and Barilla, D. (2012) Chromosome segregation in Archaea mediated by a hybrid DNA partition machine. *Proc. Natl. Acad. Sci. U.S.A.*, **109**, 3754.
35. Schumacher, M.A., Tonthat, N.K., Lee, J., Rodriguez-Castaneda, F.A., Chinnam, N.B., Kalliomaa-Sanford, A.K., Ng, I.W., Barge, M.T., Shaw, P.L. and Barilla, D. (2015) Structures of archaeal DNA segregation machinery reveal bacterial and eukaryotic linkages. *Science*, **349**, 1120–1124.
36. Barilla, D. (2016) Driving Apart and Segregating Genomes in Archaea. *Trends Microbiol.*, **24**, 957–967.
37. Zhang, H. and Schumacher, M.A. (2017) Structures of partition protein ParA with nonspecific DNA and ParB effector reveal molecular insights into principles governing Walker-box DNA segregation. *Genes Dev.*, **31**, 481–492.
38. Bartolommei, G., Moncelli, M.R. and Tadini-Buoninsegni, F. (2013) A method to measure hydrolytic activity of adenosinetriphosphatases (ATPases). *PLoS One*, **8**, e58615.
39. Otwinowski, Z. and Minor, W. (1997) Processing of X-ray diffraction data collected in oscillation mode. *Method Enzymol.*, **276**, 307–326.
40. McCoy, A.J., Grosse-Kunstleve, R.W., Adams, P.D., Winn, M.D., Storoni, L.C. and Read, R.J. (2007) Phaser crystallographic software. *J. Appl. Crystallogr.*, **40**, 658–674.
41. Adams, P.D., Afonine, P.V., Bunkoczi, G., Chen, V.B., Davis, I.W., Echols, N., Headd, J.J., Hung, L.W., Kapral, G.J., Grosse-Kunstleve, R.W. et al. (2010) PHENIX: a comprehensive Python-based system for macromolecular structure solution. *Acta Crystallogr. D. Biol. Crystallogr.*, **66**, 213–221.
42. Emsley, P., Lohkamp, B., Scott, W.G. and Cowtan, K. (2010) Features and development of Coot. *Acta Crystallogr. D. Biol. Crystallogr.*, **66**, 486–501.
43. Vollenweider, H.J., Sogo, J.M. and Koller, T. (1975) A routine method for protein-free spreading of double- and single-stranded nucleic acid molecules. *PNAS*, **72**, 83–87.
44. Ghosal, D., Trambaiolo, D., Amos, L.A. and Lowe, J. (2014) MinCD cell division proteins form alternating copolymeric cytomotive filaments. *Nat. Commun.*, **5**, 5341.
45. Jeoung, J.H., Giese, T., Grunwald, M. and Dobbek, H. (2010) Crystal structure of the ATP-dependent maturation factor of Ni, Fe-containing carbon monoxide dehydrogenases. *J. Mol. Biol.*, **396**, 1165–1179.
46. Strop, P., Takahara, P.M., Chiu, H., Angove, H.C., Burgess, B.K. and Rees, D.C. (2001) Crystal structure of the all-ferrous [4Fe-4S]₀ form of the nitrogenase iron protein from *Azotobacter vinelandii*. *Biochemistry*, **40**, 651–656.
47. Jang, S.B., Seefeldt, L.C. and Peters, J.W. (2000) Modulating the midpoint potential of the [4Fe-4S] cluster of the nitrogenase Fe protein. *Biochemistry*, **39**, 641–648.
48. Krissinel, E. and Henrick, K. (2007) Inference of macromolecular assemblies from crystalline state. *J. Mol. Biol.*, **372**, 774–797.
49. Fung, E., Bouet, J.Y. and Funnell, B.E. (2001) Probing the ATP-binding site of P1 ParA: partition and repression have different requirements for ATP binding and hydrolysis. *EMBO J.*, **20**, 4901–4911.
50. Li, C.L., Hor, L.I., Chang, Z.F., Tsai, L.C., Yang, W.Z. and Yuan, H.S. (2003) DNA binding and cleavage by the periplasmic nuclease Vvn: a novel structure with a known active site. *EMBO J.*, **22**, 4014–4025.
51. Murphy, F.V.T. and Churchill, M.E. (2000) Nonsequence-specific DNA recognition: a structural perspective. *Structure*, **8**, R83–R89.
52. Andrabi, M., Mizuguchi, K. and Ahmad, S. (2014) Conformational changes in DNA-binding proteins: relationships with precomplex features and contributions to specificity and stability. *Proteins*, **82**, 841–857.
53. DeLano, W.L. (2002) *The PyMOL Molecular Graphics System*. <http://www.pymol.org/>.
54. Soberón, N.E., Lioy, V.S., Pratto, F., Volante, A. and Alonso, J.C. (2011) Molecular anatomy of the *Streptococcus pyogenes* pSM19035 partition and segrosome complexes. *Nucleic Acids Res.*, **39**, 2624–2637.

55. Wang,X., Llopis,P.M. and Rudner,D.Z. (2013) Organization and segregation of bacterial chromosomes. *Nat. Rev. Genet.*, **14**, 191.
56. Ah-Seng,Y., Lopez,F., Pasta,F., Lane,D. and Bouet,J.Y. (2009) Dual role of DNA in regulating ATP hydrolysis by the SopA partition protein. *J. Biol. Chem.*, **284**, 30067–30075.
57. Figge,R.M., Easter,J. and Gober,J.W. (2003) Productive interaction between the chromosome partitioning proteins, ParA and ParB, is required for the progression of the cell cycle in *Caulobacter crescentus*. *Mol. Microbiol.*, **47**, 1225–1237.
58. Barilla,D., Carmelo,E. and Hayes,F. (2007) The tail of the ParG DNA segregation protein remodels ParF polymers and enhances ATP hydrolysis via an arginine finger-like motif. *PNAS*, **104**, 1811–1816.
59. Barilla,D. and Hayes,F. (2003) Architecture of the ParF*ParG protein complex involved in prokaryotic DNA segregation. *Mol. Microbiol.*, **49**, 487–499.
60. Golovanov,A.P., Barilla,D., Golovanova,M., Hayes,F. and Lian,L.Y. (2003) ParG, a protein required for active partition of bacterial plasmids, has a dimeric ribbon-helix-helix structure. *Mol. Microbiol.*, **50**, 1141–1153.
61. Radnedge,L., Youngren,B., Davis,M. and Austin,S. (1998) Probing the structure of complex macromolecular interactions by homolog specificity scanning: the P1 and P7 plasmid partition systems. *EMBO J.*, **17**, 6076–6085.